*Environment. Technology. Resources. Rezekne, Latvia*
*Proceedings of the 15th International Scientific and Practical Conference. Volume III, 440-444*

# *Obtaining a promising laser induced surface nanostructure of titanium alloy for biocompatibility*

**Edmunds Sprudzs**
Faculty of Engineering
*Rezekne Academy of Technologies*
Rezekne, Latvia
sprudzs.edmunds@gmail.com

**Lyubomir Lazov**
Faculty of Engineering
*Rezekne Academy of Technologies*
Rēzekne, Latvia
lyubomir.lazov@rta.lv

**Emil Yankov**
Faculty of Engineering
*Rezekne Academy of Technologies*
Rezekne,Latvija
emil.yankov@rta.lv

**Imants Adijans**
Faculty of Engineering
*Rezekne Academy of Technologies*
Rēzekne, Latvia
imants.adijans@rta.lv

***Abstract. Biocompatibility of materials is of paramount importance in many areas of research, engineering, medical and consumer grade product development. Biocompatibility of surfaces can be understood as resistance of the surface to harmful bacteria colonisation and subsequent biofilm creation. Traditionally, such surfaces are created by coating the base material with a different material that offers the necessary biocompatibility features. This is often not desirable, as it introduces different surface chemistry, has different physical properties than the base material, and in many cases, does not provide a lasting solution. Modification of the surface of the base material would be preferrable. In the last decade, laser ablation of surfaces to create microscale and nanoscale patterns that improve biocompatibility has been at the forefront of research in this field. This research paper provides insight into current understanding of bactericidal surface topologies and demonstrates an example of obtaining a potentially bactericidal surface of grade V titanium alloy with an industrial grade nanosecond laser.***

***Keywords: Biocompatibility, Nanotextures, Laser.***

## I. INTRODUCTION

Nanotechnology has been advancing rapidly in the last few decades. This has fostered development of surface enhancement techniques that can dramatically change surface properties and interaction with the environment. These include drag reducing, water repellent and antibacterial coatings [1], self-cleaning surfaces [2], anti-icing coatings [3] and many others.

There are two ways to alter surface properties - by changing surface chemistry or by creating physical structures on existing surfaces. Sometimes the two methods are combined to obtain a surface with desired properties.

Materials with improved antibacterial properties can have great impact on how industries like medicine, food production, processing and storage develop. Bacteria and other microorganisms attach to the surface of material and form complex multi-layered habitats protected by biofilms [4]. These structures are only partly susceptible to antibiotics, as these usually reach only the first layer with subsequent layers developing antibiotic resistance capabilities. Antimicrobial-resistant infection related deaths are expected to reach 10 million by 2050, so surfaces that prevent ab initio formation of bacteria are of high interest [5].

It has been established that micro- and nano-modifications of surfaces induce changes in cell shape and adhesion to materials [6]. Such changes include, but are not limited to changes in cell morphology, orientation, activity, behaviour, and phenotypic expression. For an example, for dental implants, preliminary research shows, that by optimising biomaterials to improve osteogenic cell proliferation, infection risks can be reduced by 60-90% without using any antibiotics [7]. The phenomenon of inducing a desired cell reaction with adequate surface structure is known as “contact guidance” and it has been observed in several cell types interacting with anisotropically patterned substrates [8]. Another term - mechano-bactericidal effect – has been used to describe capacity of nano-scale structures to physically impede and deactivate bacterial cells [9].

Several examples of this mechano-bactericidal effect are known and have been studied in nature. Wings of cicada [9] – [11] and dragonflies [12], [13] as well as feet of a gecko [14] have all been observed to show such properties. Further, it has been demonstrated that modified surfaces of materials, such as black silicon (bSi) and hydrothermally

*Print ISSN 1691-5402*
*Online ISSN 2256-070X*
*https://doi.org/10.17770/etr2024vol3.8181*

etched titanium show bactericidal properties comparable to that of their natural inspiration [15], [16].

A finite element model (FEM) to describe the mechanics of surface nanospikes rupturing bacterial cells has been developed recently by a group of scientists in Australia. An array of nanospikes with hemispherical end radius of 0.03 µm, height of 0.2 µm and centre to centre distance of 0.2 µm was used for the model and magnitude of stress and strain leading to the creep deformation of the cell wall was predicted (Fig. 1) [17].

*Fig. 1. Contour plot of the cell on nanospikes, elastic strain*

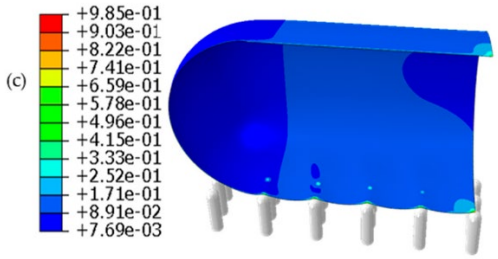


*energy density (MPa) [17].*

A practical demonstration of similar nanostructures to those derived theoretically and thus, applicability of the model referred to above has been verified on chemically etched titanium. The surface texture shown in Fig. 2 demonstrated strong bactericidal properties against *Pseudomonas aeruginosa* and *Staphylococcus aureus* cells [18].

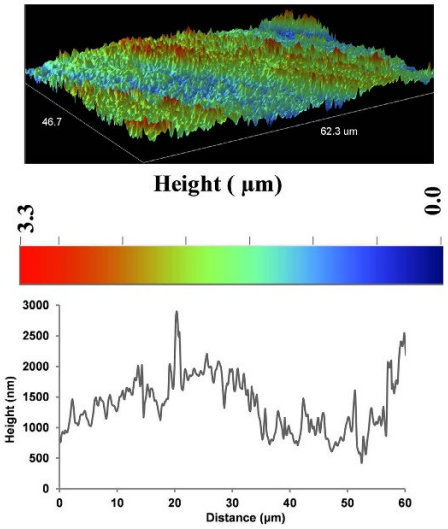


*Fig. 2. Optical profilometry images of HTE-Ti surface along with height profiles [18].*

In the current study, grade V titanium alloy surface was processed with a nanosecond laser to obtain surface nanotextures like those showing strong bactericidal properties present in nature, obtained with other surface modification technique, and those predicted mathematically.

## II. Materials and Methods

Medical grade V titanium alloy (Gr.5, Ti6-Al-4V) was selected for experiments. A sheet of 2 mm thickness was cut into 60 mm x 60 mm squares for convenient positioning under the laser for processing and under the microscope for result evaluation. No surface processing or treatment was applied prior to laser processing.

Rofin PowerLine F20 Varia dual-galvanometer laser was used for processing the samples. This is an ytterbium laser with a wavelength of 1064 nm and a pulse length down to 4 ns. The key parameters of the machine are summarized in the table below [19].

Table 1. Rofin PowerLine F20 Varia Specification

| Parameter | Value |
|---|---|
| Operating Mode | Pulsed laser |
| Wavelength | 1064 nm |
| Output Power | 0-19.7 W |
| Pulse Energy | 1 mJ |
| Pulse Width | 4, 8, 14, 20, 30, 50, 100, 200 ns |
| Repetition Rate | 20 to 1000 kHz |

Working principle of the test setup is provided in Fig. 3 [20], where a test sample is placed on the test bed and two precision mirror galvanometers direct the laser beam through an F-theta lens as set up by the user in software.

Distance between the lens and the surface of the

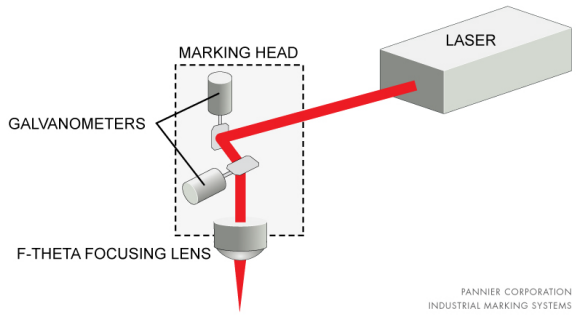


*Fig. 3. Dual-Galvanometer laser operating principle and test setup [20].*

sample can be adjusted with micrometre resolution to focus or defocus the laser beam. The focal distance of the current lens is 184 mm and laser spot size is 40 µm at this focal point. No assist gas was used, and all experiments were conducted at room temperature of about 20C.

Samples were analysed with Olympus LEXT OLS5000 3D Measuring Laser Microscope to assert the created nanostructures for compatibility with the desired topology visually as well as surface roughness was established and documented. When this analysis revealed a promising sample, additional spatial measurements were made to confirm the dimensions of surface elements and their distribution. This sample was also inspected with scanning electron microscopy (SEM) to compare the image of the structure to that of other authors.

While the exact spatial dimensions of elements and their distribution of antibacterial surfaces vary, all are in nanometre or a few micrometres scale [21]. Given the laser spot size of 40 µm, direct machining of those surface topologies is not possible with the equipment available. Thus, a strategy to produce such structures indirectly had to be found. While sources exist describing successfully creating this type of surface topology with femtosecond lasers, no documented examples were found in literature for nanosecond lasers.

Without a clear starting point, approach of matrices of

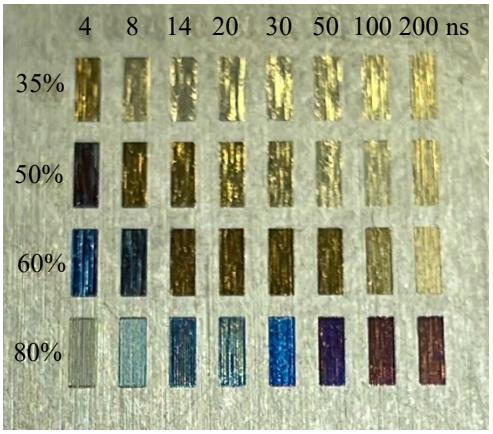


*Fig. 4. A matrix of 32 test samples.*

32 rectangles with size of 3 mm x 1 mm was chosen, were two factors of pulse width, laser power, repetition rate, scanning speed, scanning line step or angle would be altered with the remaining factors fixed. For illustration, one such matrix with varying pulse width and laser power is provided in Fig. 4. At first, cross-hatching at 90-degree angle and combined 90-degree and 45-degree angle was

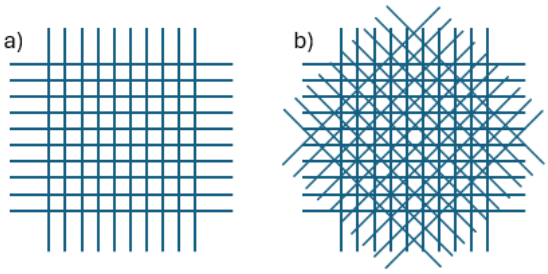


*Fig. 6. Schematic representation of hatched laser scanning patterns: a)90-degree angle, b) 90-degree and 45-degree angle.*

attempted using the entire range of laser power settings and pulse widths at a constant scanning speed of 100 mm/s (Fig. 5).

This approach did not produce the desired results. Surfaces with large, melted areas at higher energy density levels and surfaces with no visible topology change at lower energy density levels were obtained. However, sporadic appearance of desired surface structures was noticed along the scanning lines of some samples. One such example is provided in Fig. 6.

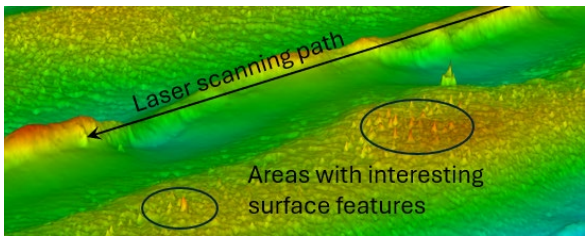


*Fig. 7. Interesting surface structures along the laser path.*

Measurements of those features were made Fig. 6 to discover they closely resemble some of the bactericidal structures found in nature discussed earlier in this paper. Rz roughness was established at close to 0.7 µm with many such features being 1 µm or closer apart. Given the chaotic nature of these features, several measurements were made to establish the scale, but visual inspection remained a key method for confirmation of suitability of the surface structure of the sample.

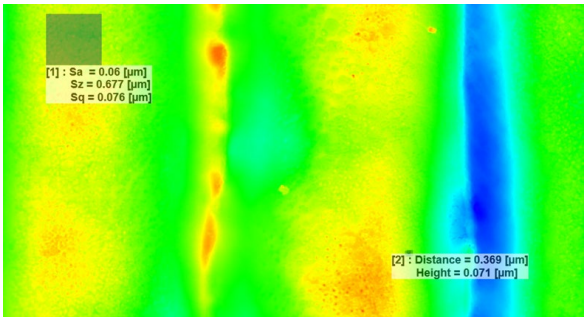


*Fig. 5. Surface roughness and distance between features.*

With this discovery, the cross-hatching strategy was dropped, and further experiments conducted in an attempt to compose the entire sample area from these "along-the-scan-line" structures. After a series of experiments, it was established that the pulse length of 4 ns was giving the most consistent features with highest structure peaks and minimum distance between features. The scanning speed was kept constant at 100 mm/s and 80% laser power setting used. Through iteration, it was established that the distance between the scanning lines of 1 µm, produced the most consistent surface structure with predominantly desirable features. Additional data and images covering the entire experiment are omitted here due to the limited number of pages available for this publication and are available on request from authors.

Effective laser radiation energy can be used to assess and compare the effect of laser processing, even when factors like pulse width, scanning speed, power and frequency differ. It is a useful measure to help put a novel approach with a different type of laser into perspective and help other researchers speed up their efforts for similar research. Laser radiation absorbed per mm$^2$ was calculated according to (1)

$$E_{eff} = \frac{APf}{v^2}, \qquad (1)$$

where $A$ is the absorption coefficient of the material, $P$ is the average power of the laser, $f$ is the repetition rate and $v$ is the laser scanning speed, respectively. While some

debate exists between scientists, it seems fair to use a constant absorption coefficient [22] of a median value of 0.4 for the given titanium alloy [23].

## III. Results and Discussion

The result of the study is a surface sample that is ready for the next step – investigation of its bactericidal properties.

It was found, that surface topology with random nanospikes with centre to centre distance between 0.1 µm and 1 µm and Rz roughness of 0.15 to 0.70, i.e. those, with spatial profile closely resembling that of bactericidal surfaces found in nature [9] – [14], obtained experimentally [15], [16], and those shown in mathematical model [17] are formed at $E_{Eff}$ close to 0.30 J/mm$^2$ with a pulse width of 4 ns. A Micrograph of the sample is provided in Fig. 8.

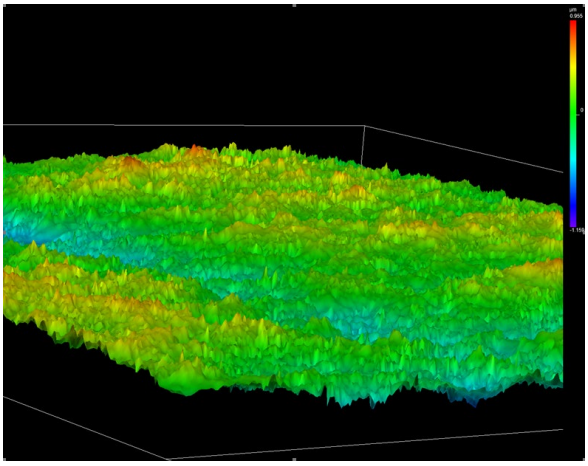

*Fig. 9. A micrograph of the surface of the sample.*

A closeup for better visualization is provided in Fig. 9. Surface roughness to assess the depth of the features and feature peak-to-peak measurements are provided in Fig. 10.

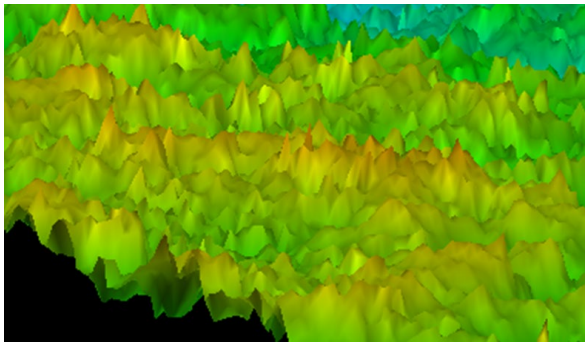

*Fig. 10. A closeup of the surface topology of the sample.*

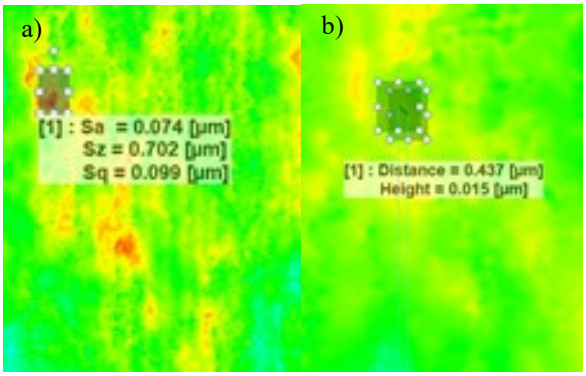


*Fig. 8. Sample measurements: (a) Surface roughness measurement, (b) feature peak-to-peak- distance measurement.*

Image of the sample at a magnification of 100x is provided in fig10.

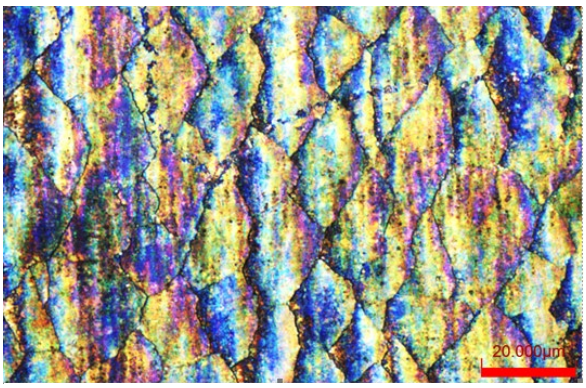


*Fig. 12. 100x image of the sample.*

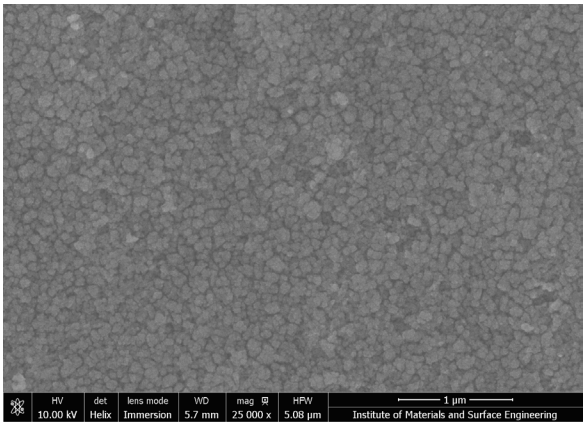


*Fig. 11. SEM image of the sample.*

SEM investigation of the achieved topology was conducted for further reference and is provided in Fig. 12.

## IV. Conclusions

This study attempted and successfully produced surface topology structures on titanium grade V alloy that based on current state of the art shall exhibit bactericidal properties. The work described in this study is the first step of a multi-step journey and provides promising grounds for further research of laser induced surface nanostructures with industrial grade nanosecond lasers as opposed to

much more complex and lab-constrained femtosecond lasers. The next step is to conduct anti-bacterial experiments to confirm reduced rates of gram-negative and gram-positive bacterial development and biofilm formation. More experiments with the resulting energy densities close to the $E_{eff}$, pulse width and scanning pattern already identified shall be conducted to finetune the surface structure response of the material and to increase the processing speed. Stereoscopic SEM imaging shall be performed to both, confirm the already established spatial dimensions of surface nanotexture profile as well as establish the effective spike hemispherical end radius and try to reduce it during future experiments. X-ray diffractometer could be used to perform analysis of the surface texture to better understand the processes governing the formation of the required nanospikes.

## REFERENCES

[1] Samaha, M. A., Tafreshi, H. V., & Gad-el-Hak, M. (2012). Superhydrophobic surfaces: From the Lotus Leaf to the submarine. Comptes Rendus Mécanique, 340(1-2), 18–34. https://doi.org/10.1016/j.crme.2011.11.002.

[2] Zhang, X., Liu, X., Laakso, J., Levänen, E., & Mäntylä, T. (2012). Easy-to-clean property and durability of superhydrophobic flaky γ-alumina coating on stainless steel in field test at a paper machine. Applied Surface Science, 258(7), 3102–3108. https://doi.org/10.1016/j.apsusc.2011.11.045.

[3] Wang, F., Li, C., Lv, Y., Lv, F., & Du, Y. (2010). Ice accretion on superhydrophobic aluminum surfaces under low-temperature conditions. Cold Regions Science and Technology, 62(1), 29–33. https://doi.org/10.1016/j.coldregions.2010.02.005.

[4] Donlan, R. M. (2002). Biofilms: Microbial life on surfaces. Emerging Infectious Diseases, 8(9), 881–890. https://doi.org/10.3201/eid0809.020063.

[5] Tripathy, A., Sen, P., Su, B., & Briscoe, W. H. (2017). Natural and bioinspired nanostructured bactericidal surfaces. Advances in Colloid and Interface Science, 248, 85–104. https://doi.org/10.1016/j.cis.2017.07.030.

[6] Curtis, A., & Wilkinson, C. (1997). Topographical control of cells. Biomaterials, 18(24), 1573–1583. https://doi.org/10.1016/s0142-9612(97)00144-0.

[7] Gasik, M., Braem, A., Chaudhari, A., Duyck, J., & Vleugels, J. (2015). Titanium implants with modified surfaces: Meta-analysis of in vivo osteointegration. Materials Science and Engineering: C, 49, 152–158. https://doi.org/10.1016/j.msec.2014.12.074.

[8] Meyle, J., Gültig, K., Brich, M., Hämmerle, H., & Nisch, W. (1994). Contact guidance of fibroblasts on biomaterial surfaces. Journal of Materials Science: Materials in Medicine, 5(6-7), 463–466. https://doi.org/10.1007/bf00058984.

[9] Linklater D.P., S. Juodkazis, E.P. Ivanova, Nanofabrication of mechanobactericidal surfaces, Nanoscale 9 (43) (2017) 16564-16585. https://doi.org/10.1039/c7nr05881k.

[10] Ivanova E.P., et al., Natural bactericidal surfaces: mechanical rupture of Pseudomonas aeruginosa cells by cicada wings, Small 8 (16) (2012) 2489-2494. https://doi.org/10.1002/smll.201200528.

[11] Kelleher S.M., et al., Cicada wing surface topography: an investigation into the bactericidal properties of nanostructural features, ACS Appl. Mater. Interfaces 8 (24) (2016) 14966-14974. https://doi.org/10.1021/acsami.5b08309.

[12] Bandara C.D., et al., Bactericidal effects of natural nanotopography of dragonfly wing on Escherichia coli, ACS https://doi.org/10.1021/acsami.6b13666.

[13] Mainwaring D.E., et al., The nature of inherent bactericidal activity: insights from the nanotopology of three species of dragonfly, Nanoscale 8 (12) (2016) 6527-6534. https://doi.org/10.1039/c5nr08542j.

[14] Li X., et al., The nanotipped hairs of gecko skin and biotemplated replicas impair and/or kill pathogenic bacteria with high efficiency, Nanoscale 8 (45) (2016) 18860-18869. https://doi.org/10.1039/c6nr05046h.

[15] Ivanova E.P., et al., Bactericidal activity of black silicon, Nat. Commun. 4 (2013) 2838. https://doi.org/10.1038/ncomms3838.

[16] Hayles A., et al., Hydrothermally etched titanium: a review on a promising mechano-bactericidal surface for implant applications, Mater. Today Chem. 22 (2021), 100622, https://doi.org/10.1016/j.mtchem.2021.100622.

[17] Islam, M., et al., Finite Element Modeling of a Gram-Negative Bacterial Cell and Nanospike Array for Cell Rupture Mechanism Study. (2023) Molecules. 28. 2184. 10.3390/molecules28052184.

[18] Bhadra, C.M., et al., Antibacterial titanium nano-patterned arrays inspired by dragonfly wings. Sci. Rep. 2015, 5, 16817, https://doi.org/10.1038/srep16817.

[19] Rofin. (2015). FIBER LASERS PowerLine F Series for Marking and Micro Processing. Bergkirchen, Germany; Rofin.

[20] Pannier Corporation. (2021, November 29). Comparison: Galvanometer vs. flatbed laser marking. Pannier Corporation. Retrieved January 18, 2023, from https://www.pannier.com/laser/flatbed-vsgalvo-lasers/.

[21] Larrañaga-Altuna, M., Zabala, A., Llavori, I., Pearce, O., Nguyen, D. T., Caro, J., Mescheder, H., Endrino, J. L., Goel, G., Ayre, W. N., Seenivasagam, R. K., Tripathy, D. K., Armstrong, J., & Goel, S. (2021). Bactericidal surfaces: An emerging 21st-century ultra-precision manufacturing and materials puzzle. Applied Physics Reviews, 8(2), 021303. https://doi.org/10.1063/5.0028844

[22] J. Yang, S. Sun, M. Brandt, W. Yan, Experimental investigation and 3D finite element prediction of the heat affected zone during laser assisted machining of Ti6Al4V alloy. J. Mater. Process. Technol., 210 (15) (2010), pp. 2215-2222, https://doi.org/10.1016/j.jmatprotec.2010.08.007.

[23] M. Keller, A. Chaudhary, S. Kelly, S. Medieros, Absorption coefficient characterization in Ti-6Al-4V laser additive manufacturing, Proceedings of ICALEO (2006), p. 1204, https://doi.org/10.2351/1.5060759.